

Supplementary Information

Facile formation of ZIF-8 thin film on ZnO nanorods

Hanan Al-Kutubi,^a Alla Dikhtiarenko,^b Hamid Reza Zafarani,^a Ernst J. R. Sudhölter,^a
Jorge Gascon,^b and Liza Rassaei^{a*}

^a Laboratory of Organic Materials and Interfaces, Department of Chemical Engineering,
Delft University of Technology
Julianalaan 136, 2628 BL Delft, The Netherlands.

E-mail: l.rassaei@tudelft.nl

^b Catalysis Engineering Section, Department of Chemical Engineering
Delft University of Technology, Julianalaan 136, 2628 BL Delft, The Netherlands

Content

Experimental.....	3
Materials and equipment.....	3
Electrochemical deposition of zinc oxide nanorod array	3
Synthesis of ZIF-8 thin film coating.....	3
Contact angle measurements	4
Quantitative determination of ZIF-8 content using PXRD data.....	4
Electrochemical Deposition of Zinc Oxide Nanorod Array.....	6
Synthesis ZIF-8 thin film.....	9
Effect of heating procedure.....	9
Effect of linker concentration	13
Effect of reaction time	14
Effect of reaction time using DMF	16
Effect of underlying zinc oxide nanorod morphology	17
References	18

Experimental

Materials and equipment

Zinc nitrate hexahydrate (99%), 2-methylimidazole (Hmin), Hexamethylenetetramine (HMT), Methanol and *N,N*-Dimethyl-formamide (DMF) were all obtained from Sigma-Aldrich. Fluorine-doped tin oxide glass (FTO) with a resistivity of $\sim 7\Omega/\text{sq}$ was obtained from Aldrich and cut into $1\text{ cm} \times 2\text{ cm}$ pieces before use. Both the platinum coil counter electrode as well as the saturated Ag/AgCl reference electrode were obtained from BASi Inc.

Samples were analysed using a JEOL JSM-6010LA scanning electron microscope (SEM), an FEI Nova NanoSEM 450 (FE-SEM) and ImageJ software. Electrochemical deposition was carried out using an Eco Chemie Metrohm AUT83987 Autolab potentiostat. Powder X-ray diffraction (PXRD) measurements were performed on the Bruker D8 Advance diffractometer with the goniometer radius 217.5 mm, 2° Soller slits, and 0.3-mm receiving slit. The PXRD patterns were recorded within an angle range 2θ of $5.0 - 80.0^\circ$ at room temperature using $\text{CoK}\alpha$ radiation ($\lambda = 1.790263\text{ \AA}$) with the following measurement conditions: tube voltage of 40 kV, tube current of 40 mA, step-scan mode with a step size of $0.0092^\circ 2\theta$, and counting time of 0.2 s/step. When required, samples were heated using a Heraeus Instrument D-63450 oven and again checked using PXRD technique.

Electrochemical deposition of zinc oxide nanorod array

Before zinc oxide deposition, pre-cut FTO glass plates were ultrasonicated in acetone, ethanol and deionized water for 10 minutes at a time. Copper tape was used to enable the connection between the potentiostat and the FTO glass. To define the surface area available for deposition, all but 1 cm^2 of FTO was masked using Teflon tape.

Zinc oxide deposition was carried out using 10 ml of an equimolar solution of zinc nitrate and HMT in deionized water. The concentrations of zinc nitrate and HMT were varied to examine their effect, yet in all cases an equimolar concentration of the two precursors was used. The solution was kept at 70°C using a water bath. A small magnetic stirrer was used to ensure uniform distribution of heat and starting materials. A three electrode setup was used with a saturated Ag/AgCl reference electrode, platinum coil counter electrode and a FTO working electrode. The current was controlled using a potentiostat. Deposition was carried out for a predetermined amount of time until a specific total charge was reached. After deposition, the sample was rinsed thoroughly with de-ionized water and dried gently under nitrogen flow.

Synthesis of ZIF-8 thin film coating

For the formation of ZIF-8, already grown zinc oxide rods (using 0.3 mA for 1.2 C) were used unless stated otherwise. A solution of linker with the desired concentration was obtained by dissolving 2-methylimidazole (Hmin) in either methanol or DMF. Of this solution, $200\text{ }\mu\text{L}$ was deposited onto the zinc oxide coated FTO glass and allowed to dry in ambient conditions. When using the pure linker, the powder was finely grounded with a mortar and pestle. In case an aluminium heating block was used, samples were placed

in glass vials which were covered with a glass petri dish lid to ensure minimal loss of linker due to evaporation. In the oven, the samples were covered with an hourglass and placed inside a closed Petri dish to reduce the risk of contamination when multiple samples were heated simultaneously. The samples were then heated to a temperature of 150 °C for a designated amount of time. After ZIF-8 formation, the samples were allowed to cool to room temperature, and then they were thoroughly washed and soaked in the solvent used for the linker dissolution to ensure full unreacted linker removal. Samples were then allowed to dry in air overnight.

Contact angle measurements

Contact angle measurements were conducted using a Krüss FM 40 EasyDrop setup with accompanying software. Three measurements were performed per sample using deionised water with a droplet volume of 14 µL. Analysis was done using the accompanying software.

Quantitative determination of ZIF-8 content using PXRD data.

The mass ratios of ZIF-8 and zinc oxide were determined *via* quantitative calculation based on the PXRD data using the PowderCell software.¹ Quantification of phase content was carried out with whole powder pattern decomposition method (WPDM) routine² where the percentage of each phase was calculated as

$$c_i = I_i \rho_i k_i \mu^* = I_i \rho_i k_i \sum c_i \mu_i^*$$

where c_i is the percentage of i -phase, ρ_i the X-ray density of i -phase, k_i the calibration coefficient of i -phase, μ^* the mass absorption coefficient of the specimen and I_i is the intensity of the peaks of i -phase. In our case, the density and mass absorption coefficient for ZIF-8 and ZnO phases were known from crystallographic information files reported previously^{3, 4} and obtained from COD^{5, 6} (#4118892)⁴ and ICSD (#0005203) databases, respectively. During the analysis of each experimental data, simulated PXRD patterns for both ZIF-8 and ZnO components was normalized according to

$$I_i = I_i^0 / (V_{uc}^2 \cdot \rho_i) = I_i^0 / (V_{uc} \cdot m_i)$$

where ρ_i is the X-ray density of i -phase, V_{uc} the unit cell volume of i -phase, m_i is unit cell mass of i -phase. Thus the weight fractions are easily determined since the scale factors are normally refined by the program and the densities can be evaluated as long as the unit cell volume and contents are known. So, the weight fraction for i -component in a mixture of n phases can be obtained from the equation:

$$W_i \% = \frac{c_{Ni}}{\sum_{i=1}^n c_{Ni}} \cdot 100\%$$

where c_{Ni} is normalized content value of i -phase and n is number of the phases.

During the WPDM procedure the scale factors for ZIF-8 and ZnO phases are calculated and their values are used for the percentage determination. The ratio of the scaling factors is used to determine the partial content of each phase within a two-phase sample (the content of FTO support didn't taken into account during the analysis). Additionally, the background function with the polynom of seventh degree, a constant peak width W , the lattice parameters of both phases, the zero shift of the powder pattern have been fitted during the analysis. Finally, for ZnO phase a preferred orientation, due to preferential particle location with respect to support, was observed and assumed to reduce the intensity of the reflection (100).

Electrochemical Deposition of Zinc Oxide Nanorod Array

Zinc nitrate and HMT were used in equimolar concentrations as this was shown to aid the formation of long, well-defined rods.^{7, 8} A constant current was used to control the total charge transferred during deposition. The effects of current density, solution concentration, and total charge transfer were examined in order to optimize their effects in the formation of long, well-defined, homogenous zinc oxide nanorods.

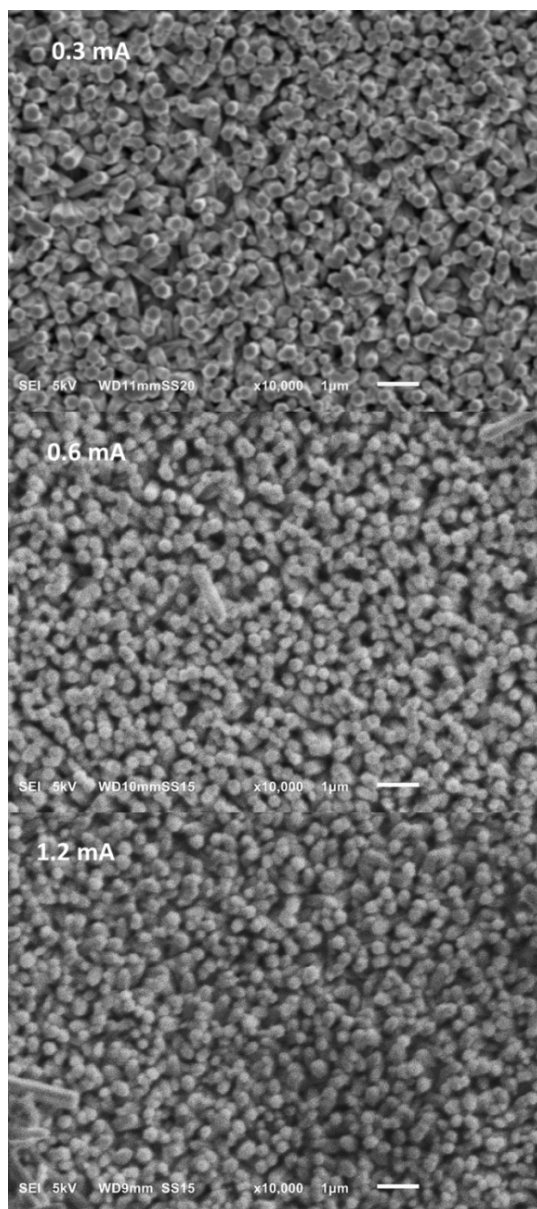


Figure S1. SEM images showing the effect of current density on zinc oxide nanorod morphology. Total charge density was 1.2 C, precursor concentration was 0.01 M. Scale bars represent 1 µm.

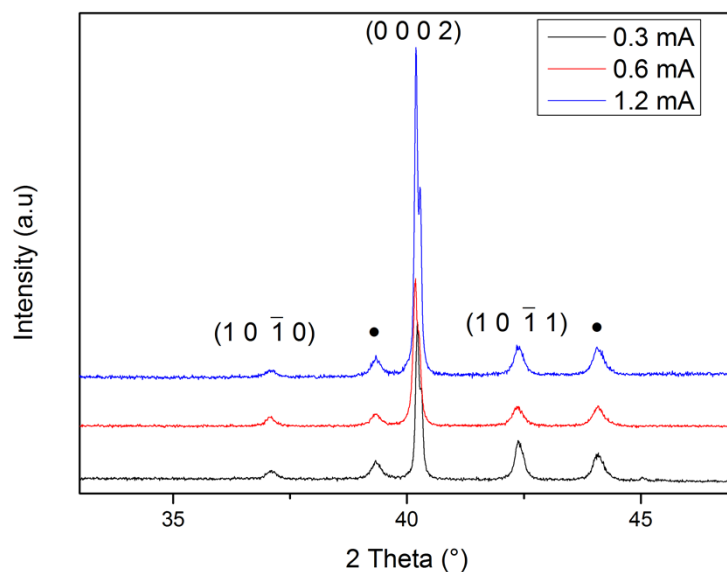


Figure S2. PXR D showing the effect of current density on zinc oxide crystal growth. The total charge density was 1.2 C, precursor concentration was 0.01 M. FTO diffraction peaks are marked by •.

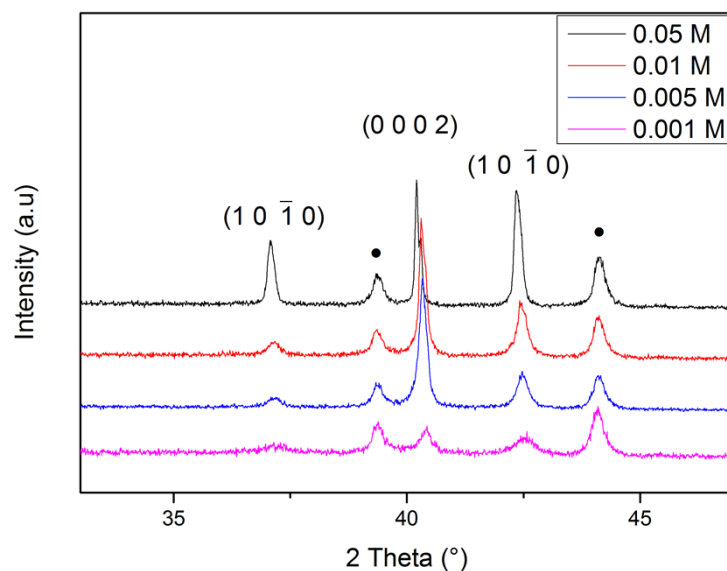


Figure S3. PXR D data showing the effect of precursor concentration on zinc oxide crystal growth. Total charge density was 1.2 C with a current density of 0.3 mA. FTO diffraction peaks are marked by •.

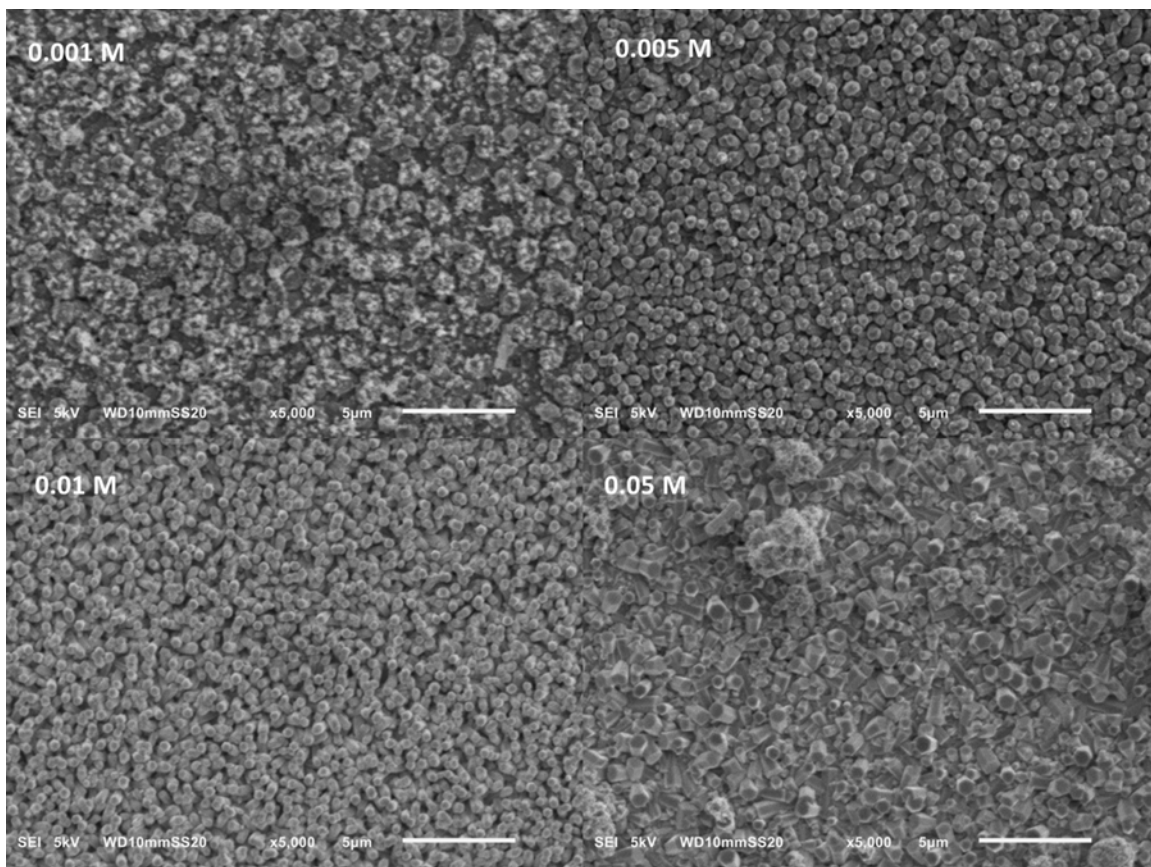


Figure S4. SEM images showing the effect of precursor concentration on zinc oxide nanorod morphology with a current density of 0.3 mA and a total charge density of 1.2 C.

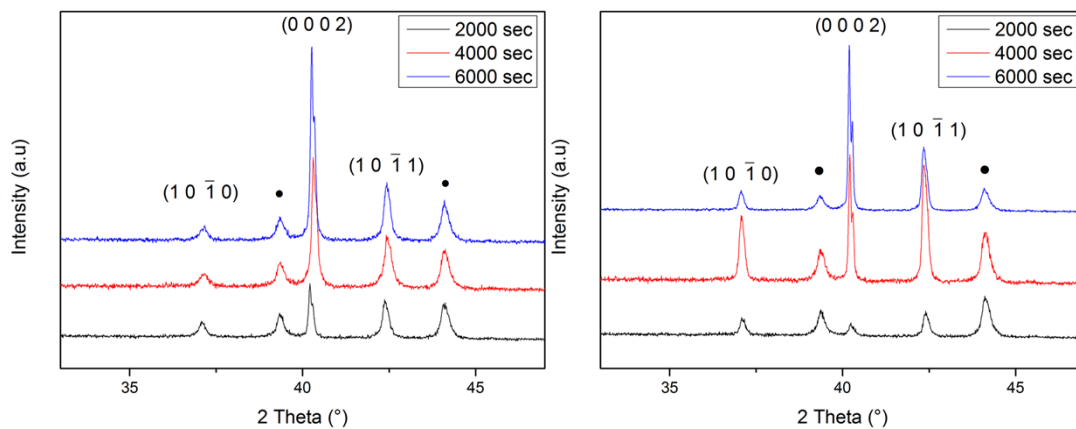


Figure S5. PXRD data showing the effect of deposition time on zinc oxide crystal growth with a current density of 0.3 mA. FTO diffraction peaks are marked by •.

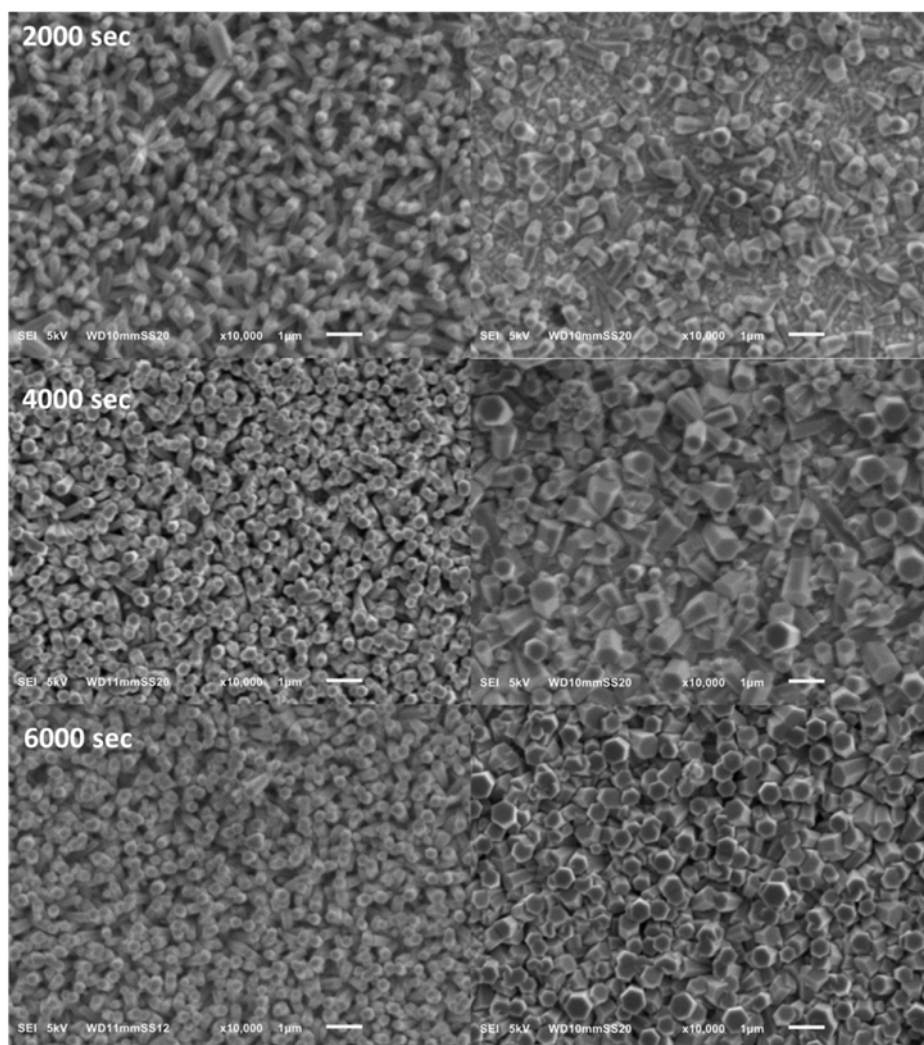


Figure S6. SEM images showing the effect of deposition time on zinc oxide morphology using a current density of 0.3 mA. The precursor concentrations were 0.01 M (left) and 0.05 M (right).

Synthesis ZIF-8 thin film

Effect of heating procedure

Both the rate of heating as well as heating method affected the ZIF-8 morphology. Heating rate had a more significant effect as shown in Figure S7 A-B. While heating the sample from room temperature to 150 °C slowly yields ZIF-8 crystals, placing the sample in a heating block already pre-heated to 150 °C yields a layer with crater-like morphology. Román *et al.* observed an increase in crystallinity and crystal size with lower heating rate,⁹ but the formation of the craters was not observed in this study. The difference between using a heating block and an oven were also examined (See Figure S7). The use of an oven results in crystals with a more narrow size distribution. This can be explained by taking linker evaporation into account. When using a heating block, samples were placed inside vials. During ZIF-8 synthesis, a large temperature gradient develops along these vials, with the bottom being much warmer than the top. The linker

therefore evaporates and sublimates on the top of the vial, effectively being lost from the reaction. Use of an oven results in a more even temperature distribution. Furthermore, using an hourglass and petri dish allow for the linker to be confined within the close vicinity of the zinc oxide (See Figure S8).

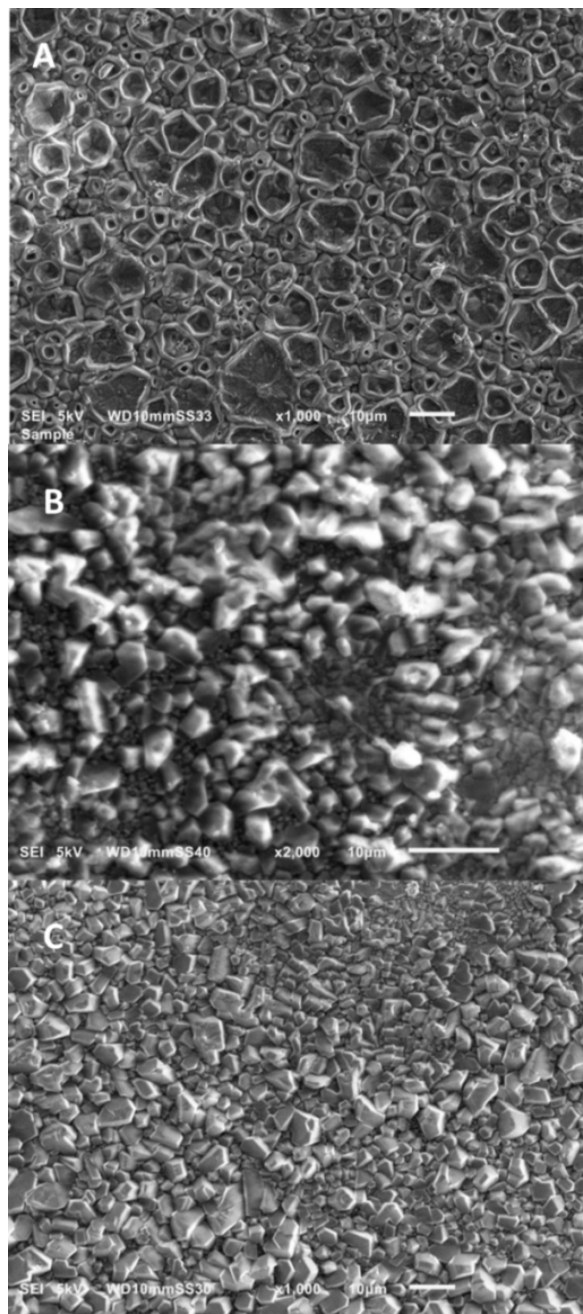


Figure S7. SEM images showing the effect of heating technique on ZIF-8 morphology. In a heating block preheated at 150 °C (A), in a heating block heated to 150 °C after sample placement (B) and heating in an oven set at 150 °C after sample placement (C).

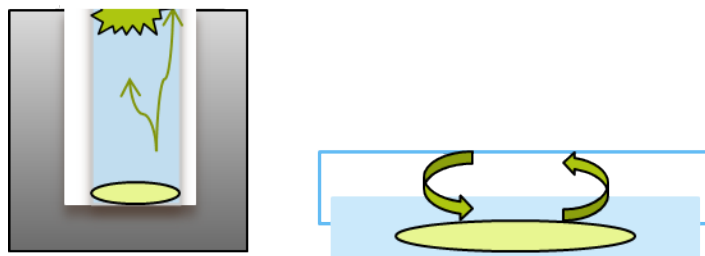


Figure S8. Schematic illustration of the effect of a heating block (left) and oven (right) on linker evaporation.

The effect of reaction time on the morphology of these craters is given in Figure S9 and Figure S10. In all cases, pure linker powder was used and samples were placed in an aluminium heating block that was pre-heated to 150 °C. Subsequent analysis using PXRD indicates the formation of ZIF-8 (See Figure S11).

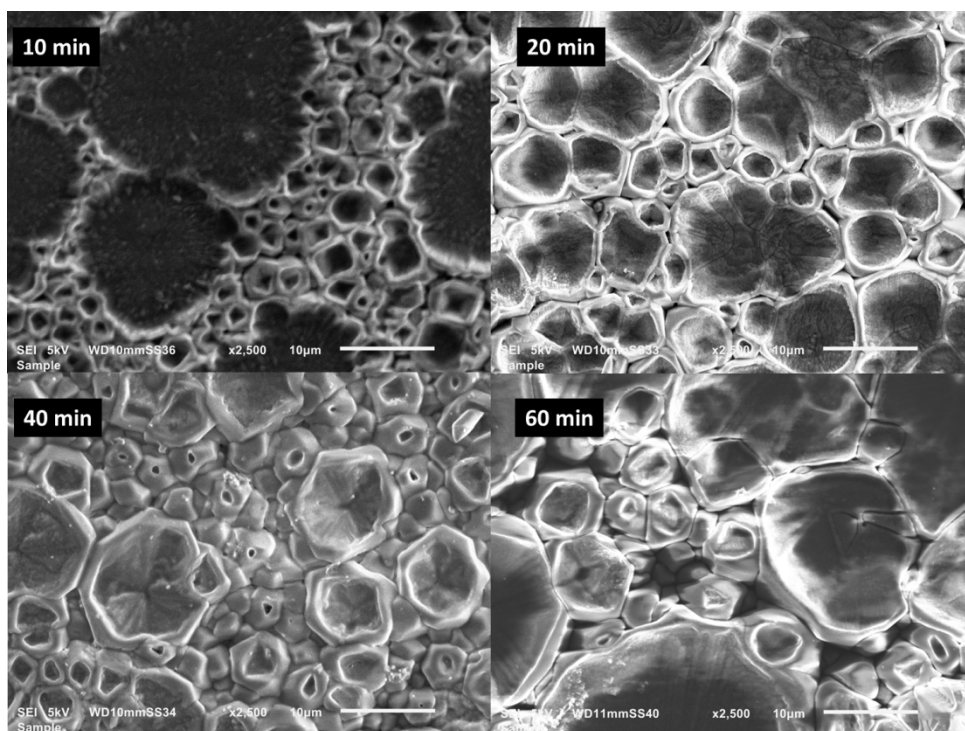


Figure S9. SEM images showing the formation of ZIF-8 with crater-like morphology with time at 2500x magnification. Pure linker powder was used and samples were placed in an aluminium heating block that was pre-heated to 150 °C.

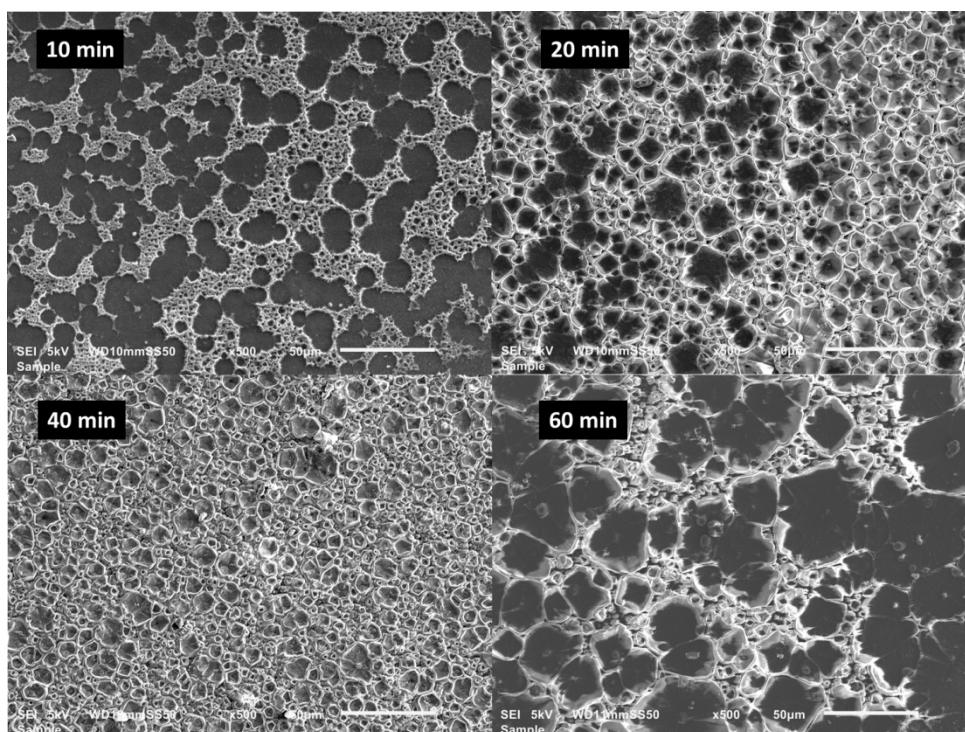


Figure S10. SEM images showing the formation of ZIF-8 with crater-like morphology with time at 500x magnification. Pure linker powder was used and samples were placed in an aluminium heating block that was pre-heated to 150 °C .

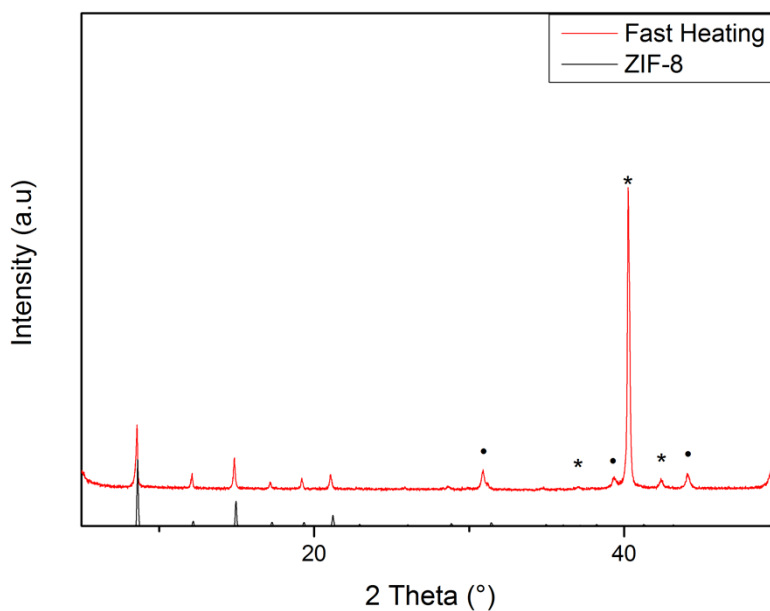


Figure S11. Comparison of PXRD diffractograms of crater-like ZIF-8 formed using a pre-heated heating block (fast heating) after 60 minutes reaction time and simulated ZIF-8 pattern (ZIF-8). Pure linker powder was used and samples were placed in an aluminium heating block that was pre-heated to 150 °C. The FTO substrate and ZnO peaks are indicated with • and *, respectively.

Effect of linker concentration

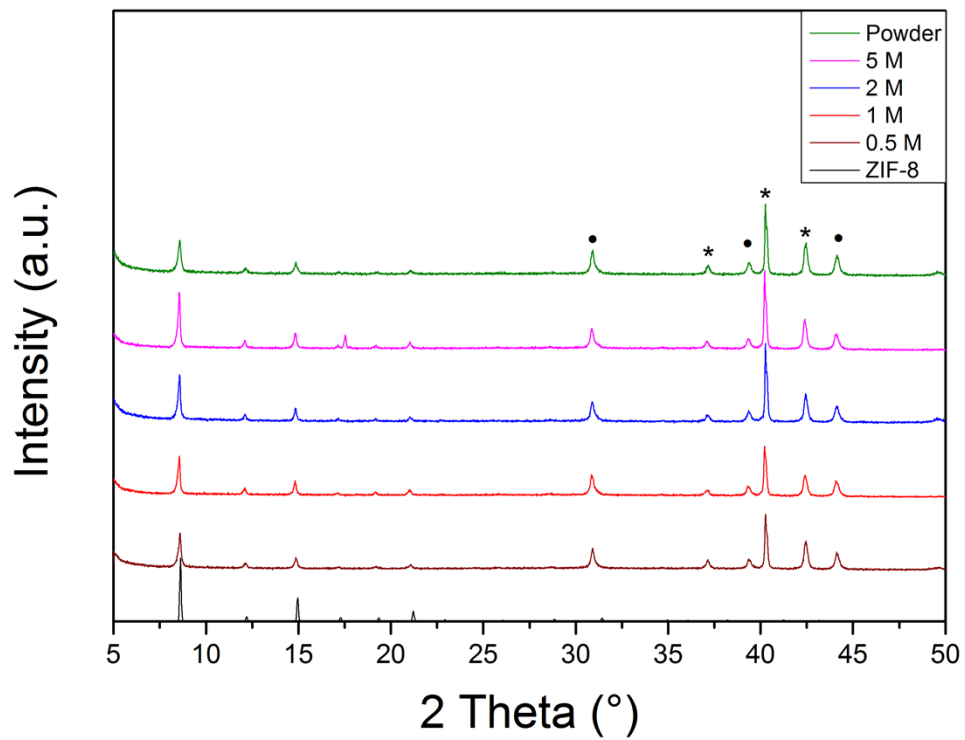


Figure S12. PXRD patterns showing the effect of linker concentration on ZIF-8 formation using methanol as solvent and after a reaction time of 20 minutes in an oven. The FTO substrate and ZnO peaks are indicated with • and *, respectively.

Effect of reaction time

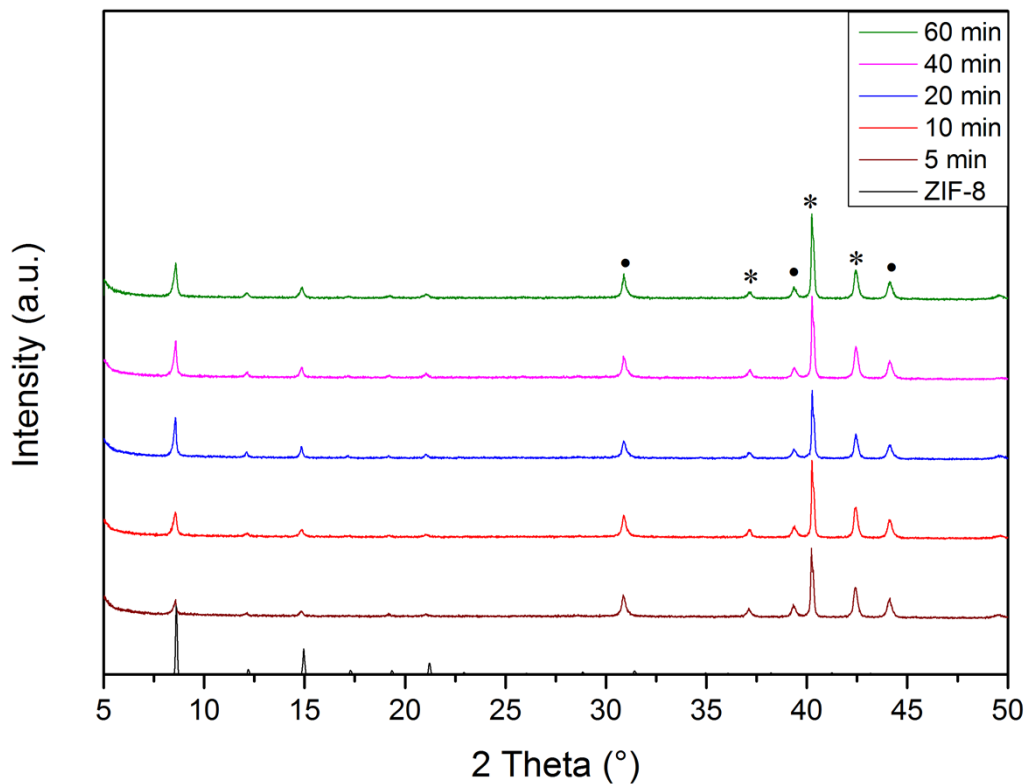


Figure S13. PXRD patterns showing the effect of synthesis time on ZIF-8 formation using a linker concentration of 2 M in methanol. Samples were heated using an oven. The FTO substrate and ZnO peaks are indicated with • and *, respectively.

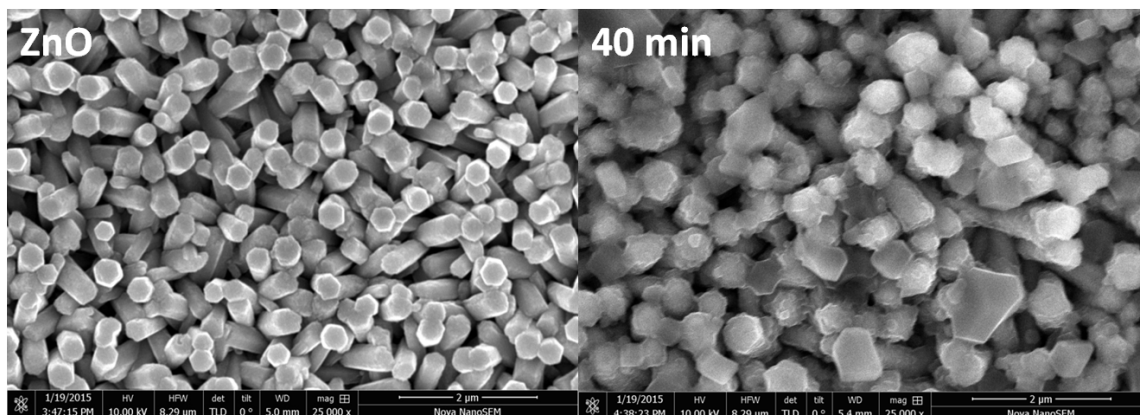


Figure S14. FE-SEM images showing the effect of reaction time on rod morphology. ZnO deposition was performed using a 0.01 M precursor concentration, a current density of 0.3 mA and a total charge of 1.2 C. For ZIF-8 formation, linker concentration was 2 M in methanol. Samples were heated using an oven.

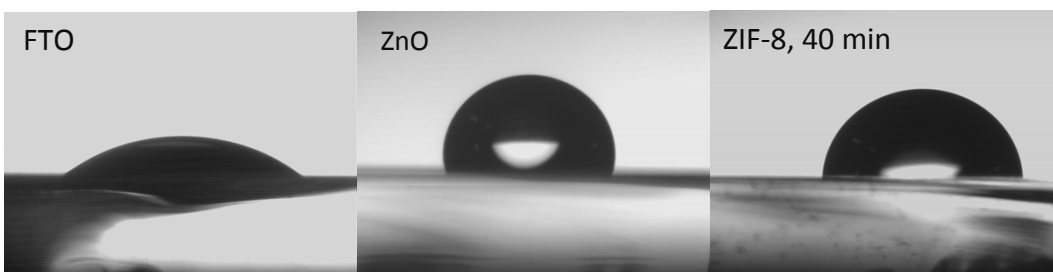


Figure S15. Contact angle measurements showing the hydrophobicity after ZnO deposition and subsequent ZIF-8 formation. ZnO deposition was done using a solution concentration of 0.01 M, 0.3 mA current density and a total charge of 1.2 C. ZIF-8 formation was done using a 2 M linker solution and methanol.

Table 1. Contact angle measurement results obtained after three individual measurements.

Sample	Measurement	Theta Left	Theta Right	Theta Median	Average
FTO	1	36.5	26.8	31.7 ± 4.87	43.83 ± 3.59
	2	52.6	63	57.8 ± 5.21	
	3	39	40.5	39 ± 0.74	
ZnO	1	109.8	104.2	107 ± 2.79	107.87 ± 1.44
	2	114.4	113	113.7 ± 0.7	
	3	102	103.7	102.9 ± 0.84	
ZIF-8 MeOH 40min	1	88.9	91.4	90.2 ± 1.27	91.27 ± 1.61
	2	88.9	91.4	90.2 ± 1.27	
	3	91.1	95.7	93.4 ± 2.29	

Contact angle can be used to assess the hydrophobicity of the sample. As can be seen, a marked increase in contact angle, and hence hydrophobicity occurs after ZnO deposition. It has been shown that for ZnO nanorods, the contact angle can vary, depending on parameters such as the amount of polar and apolar facettes exposed.¹⁰

After ZIF-8 deposition, a decrease in contact angle is observed. The reported water contact angle for ZIF-8 varies between 60° and 86°¹¹⁻¹³ and has been found to increase to 143° when the ZIF-8 possesses more hierarchal structure.¹¹

Effect of reaction time using DMF

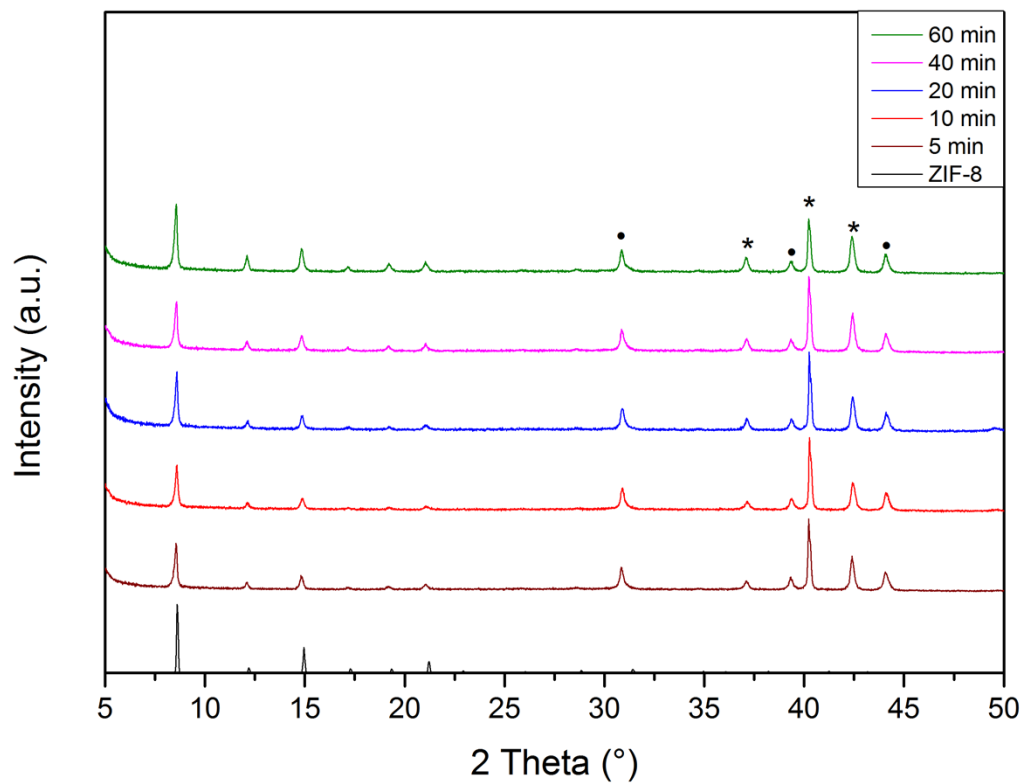


Figure S16. PXRD patterns showing the effect of synthesis time in an oven on ZIF-8 formation using a 2 M linker concentration in DMF. The FTO substrate and ZnO peaks are indicated with • and *, respectively.

Effect of underlying zinc oxide nanorod morphology

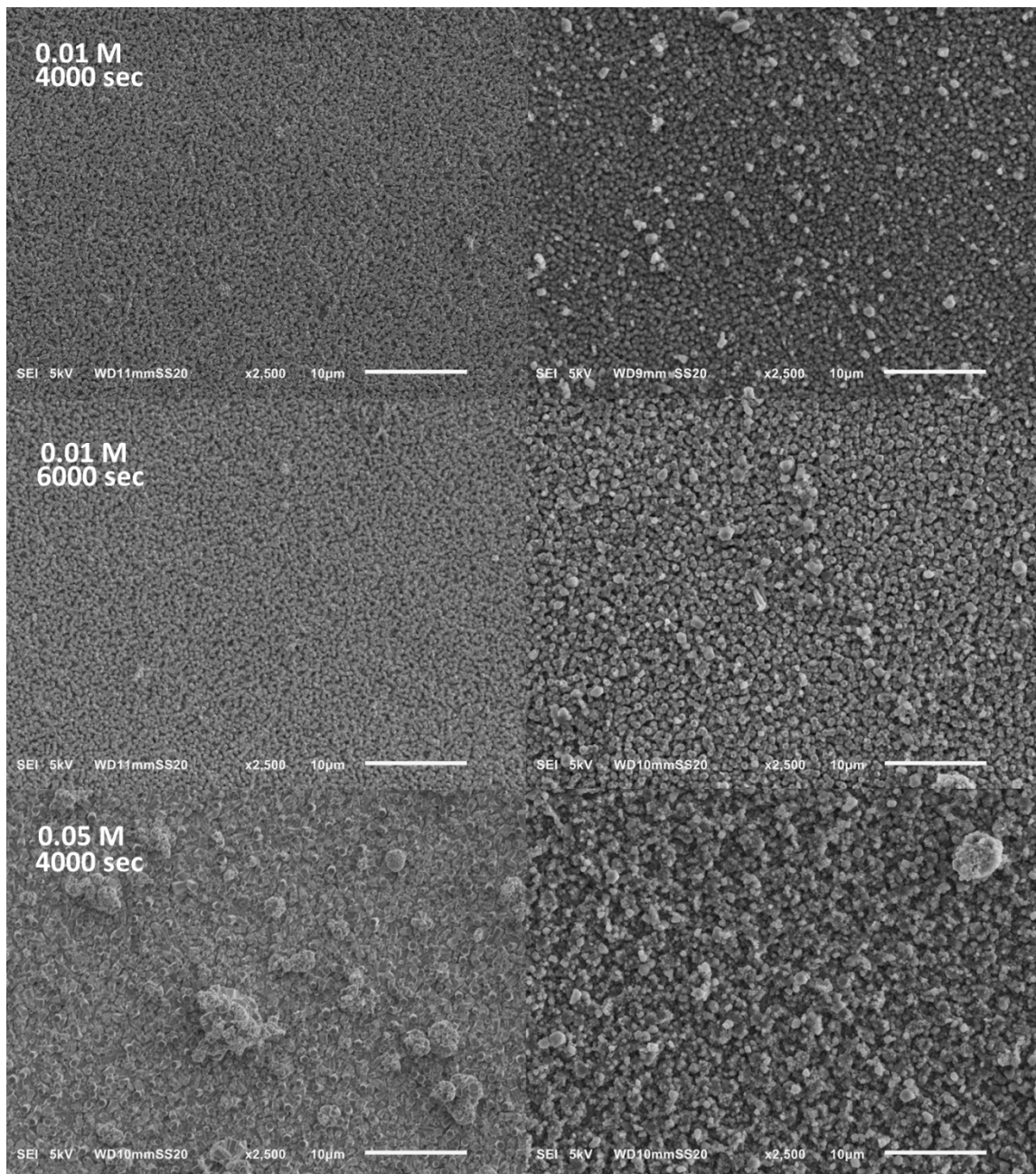


Figure S17. SEM images showing the effect of the underlying zinc oxide morphology (left) on the formation of ZIF-8 (right).

References

1. W. Krauz, *Journal of Applied Crystallography*, 1996, **29**, 301.
2. J. Martín-Ramos, A. Cambeses, A. López-Galindo, J. Scarrow and J. Díaz-Hernández, *Pathways for quantitative analysis by X-Ray diffraction*, INTECH Open Access Publisher, 2012.
3. K. Kihara and G. Donnay, *The Canadian Mineralogist*, 1985, **23**, 647-654.
4. O. Karagiari, M. B. Lalonde, W. Bury, A. A. Sarjeant, O. K. Farha and J. T. Hupp, *Journal of the American Chemical Society*, 2012, **134**, 18790-18796.
5. <http://www.crystallography.net/>.
6. C. Y. Lee, Y. S. Bae, N. C. Jeong, O. K. Farha, A. A. Sarjeant, C. L. Stern, P. Nickias, R. Q. Snurr, J. T. Hupp and S. T. Nguyen, *Journal of the American Chemical Society*, 2011, **133**, 5228-5231.
7. I. Y. Y. Bu, *Ceramics International*, 2014, **40**, 6345-6350.
8. J. Cui, *The Journal of Physical Chemistry C*, 2008, **112**, 10385-10388.
9. M. Lanchas, D. Vallejo-Sanchez, G. Beobide, O. Castillo, A. T. Aguayo, A. Luque and P. Roman, *Chemical Communications*, 2012, **48**, 9930-9932.
10. J. Lv, J. Zhu, K. Huang, F. Meng, X. Song and Z. Sun, *Applied Surface Science*, 2011, **257**, 7534-7538.
11. Y.-n. Wu, M. Zhou, B. Zhang, B. Wu, J. Li, J. Qiao, X. Guan and F. Li, *Nanoscale*, 2014, **6**, 1105-1112.
12. N. P. Panapitiya, S. N. Wijenayake, Y. Huang, D. Bushdiecker, D. Nguyen, C. Ratanawanate, G. J. Kalaw, C. J. Gilpin, I. H. Musselman, K. J. Balkus Jr and J. P. Ferraris, *Polymer*, 2014, **55**, 2028-2034.
13. X. Liu, Y. Li, Y. Ban, Y. Peng, H. Jin, H. Bux, L. Xu, J. Caro and W. Yang, *Chemical Communications*, 2013, **49**, 9140-9142.